Redistributed Pseudoinverse Control Allocation for Actuator Failure on a Compound Helicopter

Praneet Vayalali PhD Student
Michael McKay PhD Student
Farhan Gandhi Redfern Chair, Director
Center for Mobility with Vertical Lift (MOVE)
Rensselaer Polytechnic Institute
Troy, NY United States

ABSTRACT

The present study focuses on applying a redistributed pseudoinverse control allocation method on a 20,110 lb compound helicopter in order to utilize the redundant control effectors in feedback control pre- and post-actuator failure. A range of tolerable positions for locked-in-place actuator failures is established for the aircraft at a cruise speed of 150 knots. A model following linear dynamic inversion control system is implemented for the nonlinear simulation model. Stability margins, phase delay, and bandwidth evaluated for the longitudinal and lateral axis according to ADS-33E specifications show level 1 for most cases except minimum failed aft actuator position (level 2 stability margin) and maximum failed stabilator (level 3 stability margin). Nonlinear simulations are used to examine the control reconfiguration and the aircraft response for failure in the longitudinal axis (swashplate aft actuator and stabilator) and lateral axis (swashplate lateral actuator and ailerons) demonstrating the capability of the redistributed pseudoinverse method. For certain failures, especially for actuators locked in extreme positions, the post-failure response is considerably degraded (showing limit cycle oscillations, actuator saturation, or sluggish response), which was not evident from the handling qualities metrics evaluated from the extracted linear models.

NOTATION

$\vec{x}$	State Vector
$\vec{u}$	Control Input Vector
$u,\ v,\ w$	Body Velocities, ft/s
$p,\ q,\ r$	Body Angular Rates, rad/s
$\phi,\ \theta,\ \psi$	Body Roll, Pitch and Yaw Attitude, deg
$x,\ y,\ z$	Inertial Positions, ft
β_0	Rotor Coning, rad
β_{1s}	Lateral Flap, rad
β_{1c}	Longitudinal Flap, rad
β_d	Differential Flapping, rad
$\dot{\beta}_0$	Rotor Coning Derivative, rad/s
$\dot{\beta}_{1s}$	Lateral Flapping Derivative, rad/s
$\dot{\beta}_{1c}$	Longitudinal Flapping Derivative, rad/s
$\dot{\beta}_d$	Differential Flapping Derivative, rad/s
λ_0	Uniform Inflow Component
λ_{1s}	Lateral Inflow Component
λ_{1c}	Longitudinal Inflow Component
$\lambda_{0_{TR}}$	Tail Rotor Uniform Inflow
Ω	Main Rotor Rotational Speed, rad/s
θ_0	Collective Pitch, deg
θ_{1c}	Lateral Cyclic Pitch, deg
θ_{1s}	Longitudinal Cyclic Pitch, deg
θ_{ped}	Tail Rotor Collective Pitch, deg
θ_{prop}	Propulsor Feathering, deg
θ_{ail}	Aileron Deflection, deg
θ_{rud}	Rudder Deflection, deg
θ_{stab}	Stabilator Pitch Incidence, deg
s_{lat}	Lateral Actuator Position, inches
s_{fwd}	Forward Actuator Position, inches
s_{aft}	Aft Actuator Position, inches
s_{ped}	Pedal Actuator Position, inches
$M_{\theta/S}$	Mechanical Mixer
τ_p	Phase Delay, sec
ω_{BW}	Bandwidth Frequency, rad/s

Presented at the VFS International 76th Annual Forum & Technology Display, Virginia Beach, Virginia, October 6–8, 2020.

INTRODUCTION

Aircraft survivability in the event of component failure or some loss of control effectiveness is an important area of research, particularly with regards to the control system design. For fixed wing aircraft, utilization of control redundancy has been explored for enabling safe flight despite a loss or degradation in control surface performance. This work is contained largely in the Air Force's *Self-Repairing Flight Control System (SRFCS)* program, which resulted in the design and testing of a reconfigurable modified pseudoinverse type control mixer which was able to maintain trimmed flight despite failure or loss of a control surface (Refs. 1–3), as well as the *Reconfigurable Control for Tail-less Fighter Aircraft (RESTORE)* program, which highlighted the ability to reconfigure aircraft control laws when a control effector was locked-in-place (Ref. 4).

While there has been considerable work on exploitation of control redundancy for fixed-wing aircraft survivability, corresponding work in rotary-wing aircraft has been relatively limited. Hess (Ref. 5) attributes this to the lack of redundant control effectors on conventional rotorcraft. In the same work the author presents a pseudo-sliding mode control system for the UH-60A in hover, demonstrating robustness to variation in actuators, control system, vehicle characteristics, and sensors (also showing a degradation in the vehicle handling qualities). Other rotorcraft focused studies include those by Heiges (Ref. 6), where proven fixed-wing reconfiguration strategies were shown to be effective if sufficient redundancy exists in the system, as well as Enns and Si (Ref. 7), which focused on a reconfigurable swashplate control for fault tolerance.

Recently, Reddinger and Gandhi (Ref. 8) explored control reconfiguration on compound helicopters to compensate for swashplate actuator failure in trim. Vayalali et al (Ref. 9) continued this work, examining the effectiveness of the horizontal stabilator on a UH-60 Black Hawk to compensate for certain swashplate actuator locked-in-place failures. The study concludes that introducing the stabilator as a control input in the feedback loop for the control system post-failure allows the system to re-trim in flight simulation. The same group (Ref. 10) then included redundant controls in the feedback control laws for the aircraft at all times, alleviating the need for control reconfiguration post-failure, and evaluated aircraft handling qualities for such a control architecture.

For control allocation, most legacy rotorcraft utilize a control ganging method where the controls are ganged into four groups corresponding to the four control axes. This was followed in Refs. 9-10 to allocate the longitudinal authority between the main rotor swashplate and the stabilator. When multiple redundant effectors are present, as in the case of a high-speed compound helicopter, tilt-rotor, or coaxial helicopter, these effectors can be utilized to the fullest extent via an allocation method such as the pseudoinverse (Refs. 11–13). The goal of the present work is to examine the use of pseudoinverse control allocation method in feedback control and its effectiveness for different types of actuator failure.

APPROACH

Modeling

The compound helicopter configuration used in this study is based on a modified version of the UH-60A Black Hawk simulation model developed by Krishnamurthi and Gandhi (Ref. 14), which is a derivative of Sikorsky's GenHel model (Ref. 15). Validation of the UH-60A Black Hawk simulation model was performed in Ref. 14 against a trim sweep and frequency responses of flight test and GenHel data from Ref.16.

The model includes a non-linear, blade element representation of a single main rotor with articulated blades using airfoil table lookup. The blades themselves are approximated to be rigid, undergoing rotations about offset hinges. The 3-state Pitt-Peters dynamic inflow model (Ref. 17) is used to represent the induced velocity distribution on the rotor disk, while the tail rotor thrust and torque are based on the closed-form Bailey rotor (Ref. 18) with a Pitt-Peters 1-state dynamic inflow model. The rigid fuselage and empennage (horizontal and vertical tail) forces and moments are implemented as look-up tables along with wake interference factors based on wind tunnel data from the GenHel model (Ref. 15).

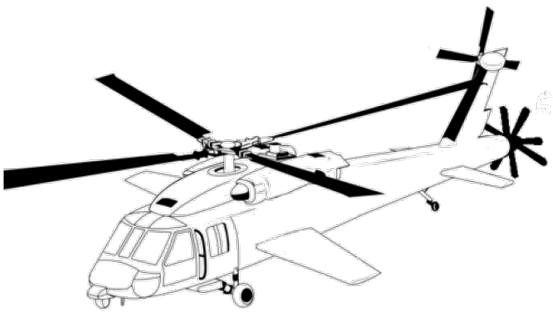

Figure 1. Compound Helicopter Schematic

The aircraft in the proposed study is a lift and thrust compounded derivative of the aforementioned UH-60A Black Hawk model so as to operate at high speeds (up to 250 knots). A fixed wing (with ailerons) and a coaxial propulsor, which is used to provide auxiliary thrust in high-speed flight, are added to the baseline helicopter (Fig. 1). Since the auxiliary thrust is provided by the propulsor, the forward shaft tilt present in the UH-60A is removed. Additionally, the Black Hawk's nonlinear blade twist is replaced by a -8° linear twist. Lowering the twist improves the aerodynamics in high-speed forward flight by reducing the negative lift and large drag on the advancing blade tips. The forces and moments of the wing are found by using Prandtl's lifting line theory, as described in Ref. 19. Interference effects between the wing and rotor are not modeled in this study as it was shown that these effects if included were shown to increase the total power by less than 1% (Ref. 20). The propulsor thrust, torque, and power is modeled using a modified version of Goldstein's vortex theory, combined with blade element theory (Refs. 19 and 21). The aircraft gross weight is raised to 20,110 lbs based on the maximum gross weight of the Piasecki X-49A Speed Hawk, which provides a reasonable approximation for the total weight of a compound aircraft with the addition of the wing, auxiliary propulsion, additional structural weight, and any other changes that must be made. Key properties of the aircraft used in the simulation are provided in Table 1 taken from Ref. 22. The aircraft nonlinear governing equations of motion are given by

$$\begin{aligned} \dot{\vec{x}} &= f(\vec{x},\vec{u}) \\ \vec{y} &= g(\vec{x},\vec{u}) \end{aligned} \tag{1}$$

where $\vec{y}$ is a generic output vector. The state vector, $\vec{x}$, is given by

$$\vec{x} = [\vec{x}_{fuselage},\ \vec{x}_{rotor},\ \vec{x}_{tailrotor}] \tag{2}$$

Table 1. Compound Helicopter Configuration Details

Parameter	Value
Gross Weight	20,110 lbs
C.G. Location	1.5 ft aft, 5.8 ft below hub
Main Rotor	
Rotor Radius	26.8 ft
Nominal Rotor Speed	258 RPM
Nominal Blade Twist	-8°
Shaft Tilt	0°
Blade Airfoils	SC-1094 R8/SC-1095
Stabilator	
Effective Area	43 ft^2
Airfoil	NACA 0012
C.P. Location	29.9 ft aft, 5.9 ft below hub
Wing	
Effective Area	226 ft^2
Mean Chord	5 ft
Aspect Ratio	9.0
Taper Ratio	0.825
Incidence Angle	1.25°
C.P. Location	0.5 ft aft, 6.5 ft below hub
Auxiliary Propulsor	
Radius	4.5 ft
Speed	1,934 RPM
Solidity	0.12
Number of Blades	4 × 2
Efficiency (150 - 250 kts)	0.80-0.87
Location	32.6 ft aft, 5.9 ft below hub

The state vector comprises of :

$$\begin{aligned} \vec{x}_{fuselage} &= [u,v,w,p,q,r,\phi,\theta,\psi,x,y,z] \\ \vec{x}_{rotor} &= [\beta_0,\beta_{1s},\beta_{1c},\beta_d,\dot{\beta}_0,\dot{\beta}_{1s},\dot{\beta}_{1c},\dot{\beta}_d,\lambda_0,\lambda_{1s},\lambda_{1c}] \\ \vec{x}_{tailrotor} &= [\lambda_{0_{TR}}] \end{aligned} \quad (3)$$

The control input vector for the aircraft model is given by

$$\vec{u} = [\theta_{1c},\theta_{1s},\theta_0,\theta_{tr},\theta_{prop},\theta_{ail},\theta_{rud},\theta_{stab}]^T \quad (4)$$

For designing the control laws, the full 24-state linear model is reduced to an 8-state quasi-steady model whose state vector is given by

$$\vec{x}_r = [u,v,w,p,q,r,\phi,\theta]^T \quad (5)$$

Swashplate Actuator Geometry

Collective, lateral and longitudinal blade pitch $(\theta_0,\theta_{1c},\theta_{1s})$ are achieved by moving the base of the pitch link from the reference plane of the level swashplate. The non-rotating swashplate orientation is fully defined by the height of the swashplate servo actuators $(s_{lat},s_{fwd},s_{aft})$ which actuate to transmit pilot control, as shown in Fig. 2. The servo actuator positions are related to the blade pitch controls $(\theta_0,\theta_{1c},\theta_{1s})$ by Eqs. 6-11 where $k_1 = 11.34$ and $k_2 = 7$. These relationships demonstrate that the independent control of θ_0, θ_{1c}, and θ_{1s} is attainable with full control of s_{lat}, s_{fwd}, and s_{aft}.

$$\theta_{1c} = \frac{k_1(s_{fwd}+s_{aft})}{2} - k_1 s_{lat} \quad (6)$$

$$\theta_{1s} = k_1\frac{(s_{fwd}-s_{aft})}{2} \quad (7)$$

$$\theta_0 = k_2\frac{(s_{fwd}+s_{aft})}{2} \quad (8)$$

$$s_{lat} = \frac{k_1\theta_0 - k_2\theta_{1c}}{k_1k_2} \quad (9)$$

$$s_{fwd} = \frac{k_1\theta_0 + k_2\theta_{1s}}{k_1k_2} \quad (10)$$

$$s_{aft} = \frac{k_1\theta_0 - k_2\theta_{1s}}{k_1k_2} \quad (11)$$

To produce an increase in collective pitch (θ_0) without changing the cyclic pitches, all three actuators need to be raised the same amount. Isolated increases in longitudinal cyclic pitch (θ_{1s}) result from a differential between the forward and aft actuators, while isolated lateral cyclic pitch (θ_{1c}) variation is accomplished by changing the lateral actuator position.

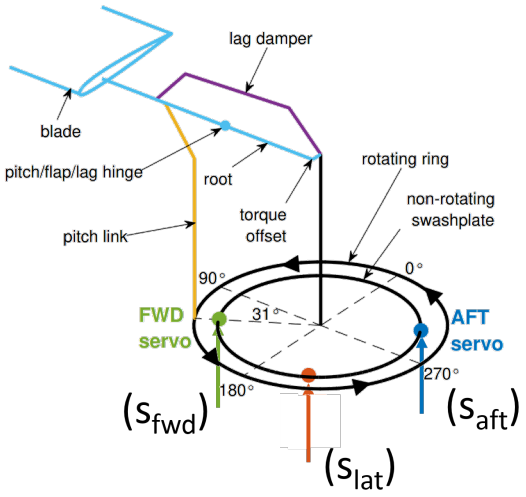

Figure 2. Swashplate Servo Actuator Geometry

The servo naming convention is given relative to the primary effect that each actuator has on the flapping of the rotor (Fig. 2). Increases in the forward actuator height will increase longitudinal cyclic pitch and the rotor will tilt back, increases in the lateral actuator height will decrease lateral cyclic pitch and rotor will tilt left side up, and increases in the aft actuator height will reduce longitudinal cyclic pitch and the rotor will tilt forward.

Servo Actuator Failure

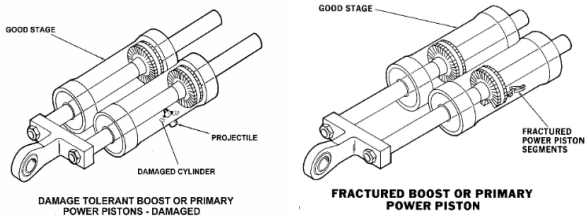

Figure 3. Actuator Failure Modes (Ref. 23)

Figure 3 from Ref. 23 shows the two modes of failure expected in a hydraulic servo actuator. A breach of the hydraulic chamber would cause pressure loss to the actuator and result

in a floating piston position as dictated by the rotor aerodynamic loading. The second failure type involves a piston jam within the cylinder such that the servo position is fixed. This is the type of actuator failure addressed in the present study, referred to as a *locked condition*, where the input signal to a control actuator yields no response, as the actuator position is locked in place. This type of actuator failure at the swashplate level results in a loss of independent control of the three blade pitches $(\theta_0, \theta_{1c}, \theta_{1s})$ as seen in Eqs. 6-11. Independent control of one is possible (over a certain range), but the two remaining blade pitches are governed by a constraint equation. For example, in the case of s_{fwd} or s_{aft} locked in place, lateral cyclic pitch (θ_{1c}) remains independently controllable (by use of s_{lat}), while longitudinal cyclic (θ_{1s}) and collective pitch (θ_0) become coupled. However, this loss of independent control can be mitigated through the inclusion of the redundant control effectors in the feedback loop throughout operation. In the present study, the redundant control effectors $(\theta_{prop},\ \theta_{ail},\ \theta_{rud},\ \theta_{stab})$ are allocated along with rotor collective and cyclic pitch $(\theta_0, \theta_{1c}, \theta_{1s})$ for all of the relevant control axes, using the pseudoinverse control allocation method, which will be discussed in detail in a later section.

Control System Design

The control system for the simulation model is designed based on model-following linear dynamic inversion (DI) (Ref. 24). Model-following concepts are widely used in modern rotorcraft control systems for their ability to independently set feed-forward and feedback characteristics. The DI controller schedules the model with flight condition to eliminate the need for feedback gain scheduling due to similar error dynamics over different flight regimes. The controller is therefore applicable to a wide range of flight conditions (Refs. 24, 25). In the inner loop, the response type to pilot input is designed for Attitude Command Attitude Hold in the roll and pitch axes, where pilot input commands a change in roll and pitch attitudes $(\Delta\phi_{cmd}$ and $\Delta\theta_{cmd})$ and returns to the trim values when input is zero. The heave axis response type is designed for Rate Command Altitude Hold, where pilot input commands a change in rate-of-climb and holds current altitude when the commanded rate-of-climb is zero. The yaw axis response type is designed for Rate Command Direction Hold, where pilot input commands a change in yaw rate and holds current heading when the yaw rate command is zero.

The response type for the outer loop is Translational Rate Command, Position Hold, where pilot inputs command a change in ground speed and hold current inertial position when inputs are zero. With the implementation of the outer loop, the pilot input does not directly command $\Delta\phi_{cmd}$ *and* $\Delta\theta_{cmd}$ as in the inner loop control law (CLAW). Rather, they are indirectly commanded through the desired ground speeds.

Redistributed Pseudoinverse Control Allocation

The pseudoinverse provides a linear solution for the desired accelerations while minimizing the L_2 norm of the control input vector, u_{cmd}. This type of allocation is typically used for an over-actuated system such as a compound helicopter with redundant actuators. A detailed description of the pseudoinverse control allocation is available in Refs. 12, 26 and 27. Usually in a dynamic inversion control system, the matrix CB is square and invertible but for the case of overactuated systems, where CB is not square but is full row rank (meaning the matrix has more columns than rows, as in the case of redundant actuators), a pseudoinverse can be applied. The form of the pseudoinverse is as follows:

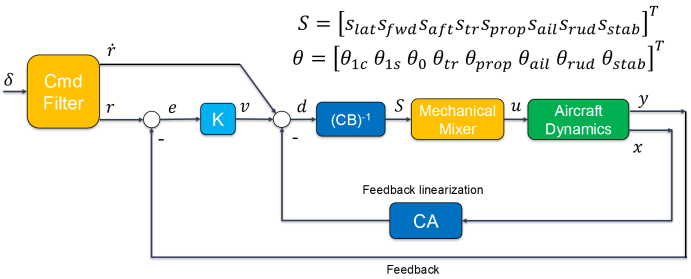

Figure 4. Dynamic Inversion Control Architecture

$$u_{cmd} = (CB)^T((CB)(CB)^T)^{-1}d \tag{12}$$

where u_{cmd} is the control command vector to the actuators, and d is the desired acceleration vector. The control sensitivity matrix, B (which is calculated from an off-line trim routine), relates the control inputs (Eq. 4) to the accelerations. In the present study, the pseudoinverse method maps the accelerations to the actuators rather than the control inputs (Eq. 4) so that actuator failure can be accounted for in the actuator space. Instead of using the control sensitivity matrix (B) a control actuator sensitivity matrix $(\hat{B})$, is defined as shown in Eq. 13.

$$\hat{B} = BM_{\theta/S} \tag{13}$$

Using Eq. 13 in Eq. 12 gives:

$$S_{cmd} = (C\hat{B})^T((C\hat{B})(C\hat{B})^T)^{-1}d \tag{14}$$

where $S_{cmd} = [s_{lat}, s_{fwd}, s_{aft}, s_{ped}, s_{prop}, s_{ail}, s_{rud}, s_{stab}]^T$, and $M_{\theta/S}$ is the mechanical mixer which represents the mechanical rigging between the actuators (S) and the control effectors $(\vec{u})$. It is important to note that for the outer loop DI controller, the forward speed is mapped to both the pitch attitude and propulsor (because the coaxial propulsor has sensitivity with only the forward acceleration in the body axis).

For the baseline compound helicopter, the pseudoinverse control allocation method provides a solution to Eq. 14 such that the actuator input vector (S_{cmd}) has a minimal L_2 norm. In the event of failure, assuming that fault detection has taken place, the column in $\hat{B}$ corresponding to the failed actuator is set to zero and the pseudoinverse is recalculated. This results in the redistribution of the controls in order to meet the desired set of accelerations without utilizing the failed actuator. In the case of forward swashplate actuator failure, this method results in a solution such that the longitudinal authority is redistributed to the aft swashplate actuator and the stabilator;

for lateral swashplate actuator failure, the lateral authority is redistributed primarily to the ailerons.

RESULTS & DISCUSSION

At a cruise speed of 150 knots, the notional (nose-level) trim of the compound helicopter is given in Table 2.

Table 2. Nominal Trim at 150 Knots

Parameter	Value
Lateral Cyclic Pitch, θ_{1c}	-2.1°
Longitudinal Cyclic Pitch, θ_{1s}	-3.4°
Collective Pitch, θ_0	9.6°
Tail Rotor Collective Pitch, θ_{tr}	8.2°
Propulsor Collective Pitch, θ_{prop}	22.6° (2061 lb_f)
Ailerons, θ_{ail}	-0.5°
Rudder, θ_{rud}	0°
Stabilator, θ_{stab}	3°
Roll Attitude, ϕ	1.4°
Rotor Lift Share	65%
Wing Lift Share	30%

The steady-state trim solution is produced by an offline trim routine using Newton-Raphson method. For a conventional helicopter, the six trim variables (collective pitch, lateral cyclic pitch, longitudinal cyclic pitch, tail rotor pitch, and vehicle pitch and roll attitudes) provide a unique solution for the six vehicle equilibrium equations. For a compound helicopter, a number of additional control variables are available. Here the pseudoinverse is utilized to calculate the next step in the trim routine because of the presence of redundant controls. The resulting solution is one out of a family of solutions that can be found by parametrically varying the redundant controls. In case of an actuator failure, a trim solution can still be found using the pseudoinverse as long as sufficient redundancy exists.

Table 3. Range of Allowable Failures at 150 knots

Parameter	Trim position	Min	Max
s_{lat}	0.81 in	-0.5 in	1.55 in
s_{fwd}	0.48 in	0 in	0.78 in
s_{aft}	-0.63 in	-1.56 in	1.2 in
s_{tr}	1.51 in	-1.6 in	1.9 in
θ_{ail}	-0.5°	-2.1°	2.2°
θ_{rud}	0°	-1°	7.5°
θ_{stab}	3°	-6.1°	10°

Table 3 shows the range of allowable actuator failures at a cruise speed of 150 knots with careful consideration of minimum blade flapping and main rotor control limits as constraints (Table 4). Here, the failed actuator/control effector setting is varied parametrically and the pseudoinverse trim routine is used to solve for the rest of the controls. Note that the allowable ranges for the aerosurfaces (θ_{ail}, θ_{rud}, & θ_{stab}) are less than the geometric limits (not shown here), which is due to the swashplate geometric limits (main rotor controls) and the minimum blade flapping limits being active at these presented values (Table 4). This implies that the rotor is incapable of compensating the moments generated by the aerosurfaces beyond the established ranges for conditions with sufficient dynamic pressure.

Table 4. UH-60A Main Rotor Control and Flapping Limits (Ref. 15)

Constraint	Limits
Collective Pitch	$0.4^\circ \leq \theta_{75} \leq 16.4^\circ$
Lateral Cyclic Pitch	$-8^\circ \leq \theta_{1c} \leq 8^\circ$
Longitudinal Cyclic Pitch	$-16^\circ \leq \theta_{1s} \leq 16^\circ$
Blade Flapping	$-6^\circ \leq \beta \leq 22^\circ$

Handling Qualities

The gains for the model-following linear dynamic inversion controller (as described in the control system design section) are tuned such that the undamaged baseline aircraft have stable closed loop poles, meet the minimum crossover frequency, gain and phase margin and range of integrator-to-proportional gain ratio requirements while minimizing over the crossover frequency (Ref. 25). For this study, the longitudinal and lateral axes are primarily taken into consideration.

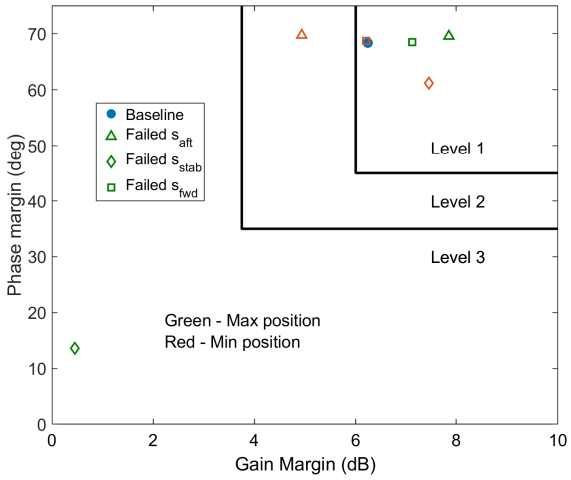

Figure 5. Pitch Axis Stability Margins

Upon establishing the allowable range of actuator failures it is important to consider the response of the aircraft during such extreme failure scenarios. Standard design practice requires 6 dB gain margin and 45° of phase margin (Ref. 28). Figure 5 shows the pitch axis gain and phase margins for the baseline undamaged aircraft (blue circle marker) along with failed forward (s_{fwd}), aft (s_{aft}), and stabilator (s_{stab}) actuators represented by the square, triangle and diamond markers, respectively, with the green and red colors showing the allowable minimum and maximum locked-in-place failure cases for each actuator. Most of the failed cases along with the baseline undamaged aircraft meet the level 1 requirement for the gain

and phase margins with the exception of minimum allowable failed aft actuator position (red triangle in level 2) and failed stabilator at the maximum allowable position in level 3 (green diamond).

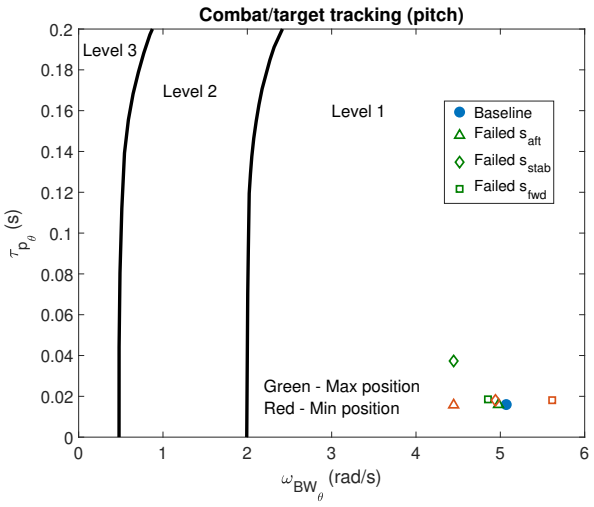

Figure 6. Pitch Axis Delays and Bandwidth

For these cases, pitch axis combat/target tracking and acquisition handling qualities ratings are also generated (Fig. 6) according to ADS-33E requirements in forward flight (Ref. 29). Figure 6 shows the pitch axis bandwidth and phase delay for the baseline and different failure cases at a cruise speed of 150 knots. As in Fig. 5, the blue marker represents the baseline undamaged aircraft while failed forward, aft, and stabilator actuators are shown by the square, triangle, and diamond markers, respectively, with the green and red colors showing the allowable minimum and maximum locked-in-place failure cases for each actuator. Overall, the handling qualities ratings for pitch axis bandwidth and phase delay fall in level 1 for all cases considered, both pre- and post-actuator failure with no significant changes in predicted aircraft performance.

Figure 7 shows the roll axis gain and phase margin (according to Ref. 28) for the baseline undamaged aircraft (blue circle marker) along with failed lateral and aileron actuators represented by the triangle and diamond markers, respectively, with the green and red colors showing the allowable minimum and maximum locked-in-place failure cases for each actuator. Here, all the cases meet the level 1 requirement for gain and phase margin with some degradation in margins for some of the failed scenarios.

Similarly, the roll axis target tracking and acquisition handling qualities ratings are also evaluated (Fig. 8) according to ADS-33E requirements in forward flight (Ref. 29). Figure 8 shows the roll attitude bandwidth and phase delays for the baseline and different failure cases at a cruise speed of 150 knots. As with Fig. 7, the blue marker represents the baseline undamaged aircraft, while failed lateral and aileron actuators are shown by the triangle and diamond markers, respectively, with the green and red colors showing the allowable minimum

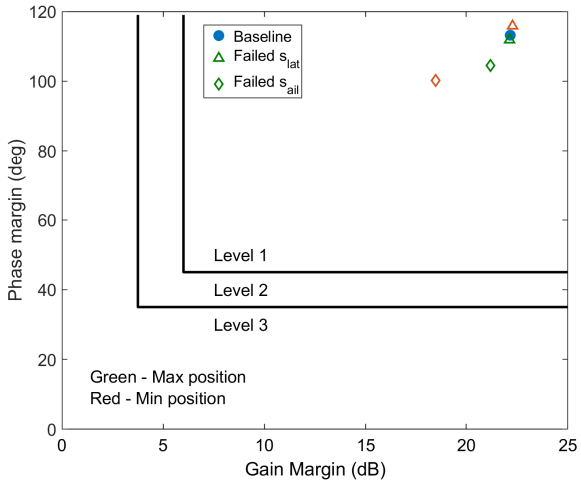

Figure 7. Roll Axis Stability Margins

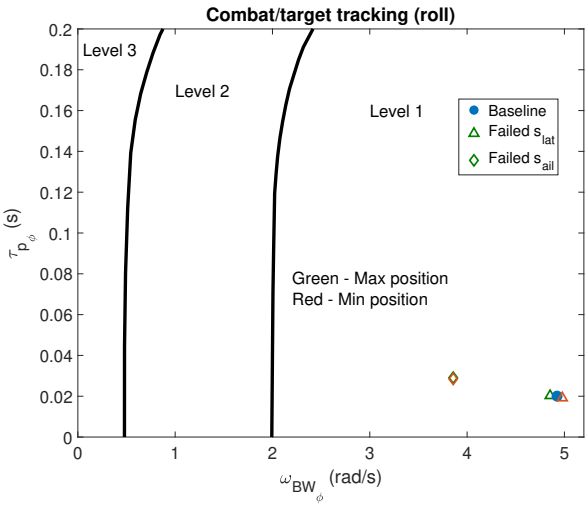

Figure 8. Roll Axis Delays and Bandwidth

and maximum locked-in-place failure cases for each actuator. It can be noted that the aircraft retains level 1 handling qualities rating for all the considered cases with some degradation in the bandwidth in the case of failed aileron actuator.

Now that the handling qualities have been established for the aircraft under different actuator fault scenarios, examining the aircraft response to these faults with the use of the redistributed pseudoinverse control allocation is important. The following results are based on the nonlinear simulation of the aircraft, as described in the modeling section, at a cruise speed of 150 knots.

Aft Actuator Failure

Failure in the aft actuator (s_{aft}) is modeled by raising the actuator by 0.3 inches and locking it in position. Figure 9a represents the time histories of the main rotor swashplate lateral, forward, and aft actuator positions from 0 to 30 seconds at 150 knots with the failure introduced at 10 seconds. From 0 to 10 seconds, the trim positions of the three actuators at 150 knots

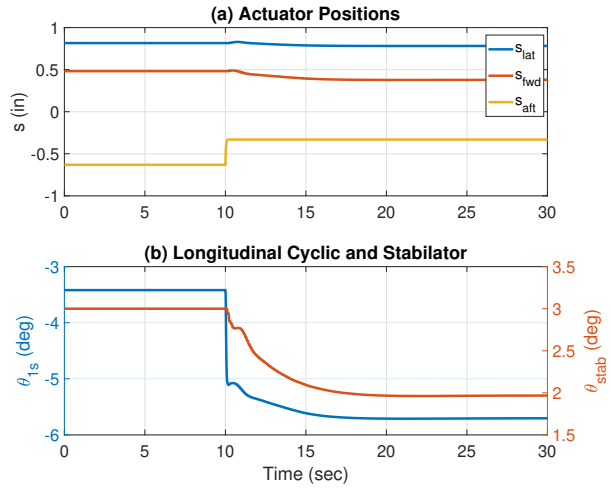

Figure 9. Time History of Actuator Positions, Longitudinal Cyclic and Stabilator for Aft Actuator Failure

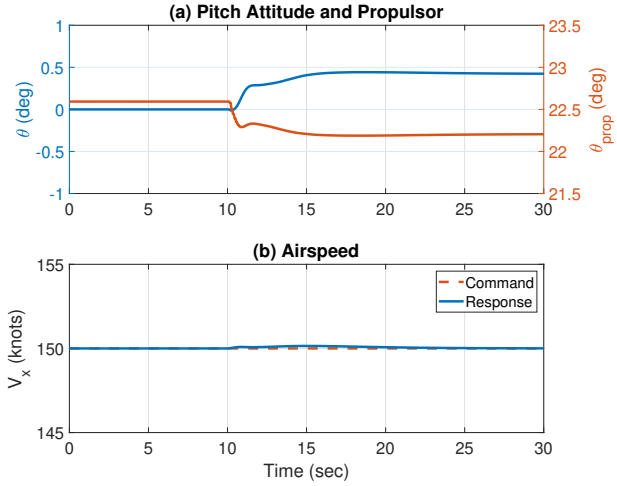

Figure 10. Time History of Pitch Attitude and Forward Velocity for Aft Actuator Failure

are shown, at 10 seconds, the aft actuator (s_{fwd}) is moved by 0.3 inches and locked out of trim. Post-failure, the forward actuator (s_{fwd}) decreases to new trim position with no substantial change in the lateral actuator (s_{lat}). Figure 9b shows the time history of the longitudinal cyclic on the left axis and the stabilator pitch incidence on the right axis. The increase in the aft actuator position along with reduction in forward actuator position results in the longitudinal cyclic (θ_{1s}) becoming more negative (-3.5° to -5.7°, solid blue line in Fig. 9b) which induces a nose-down pitching moment from the main rotor.

At 10 seconds, assuming fault detection has taken place, the pseudoinverse is recalculated in order to account for the failed actuator. As mentioned in the previous section, the redistributed pseudoinverse reallocates the pitch authority to the forward actuator and the stabilator. Hence, the stabilator is pitched leading edge down from 3° to 2° (solid red line in Fig. 9b) to produce a compensatory nose-up pitching moment. A forward reorientation of the main rotor thrust (relative to the rotor hub) due to the change in the longitudinal cyclic (θ_{1s}) also increases the propulsive force from the main rotor. In order to maintain the propulsive force, the vehicle orients itself to a slightly more nose-up pitch attitude (0° to 0.4°). In parallel to this, the propulsor feathering changes from 22.6° to 21° (solid red line in Fig. 10a) in order to maintain the airspeed (solid blue line in Fig. 10b).

Maximum vs Minimum Tolerable Failures

Figures 11 and 12 show simulations of the maximum and minimum allowable positions of the failed aft actuator according to the steady-state trim solutions at a cruise speed of 150 knots (Table 3). Consider the case of failure at the maximum aft actuator position (Fig. 11). At 10 seconds, the failure is simulated by moving the aft actuator by 1.83 inches to its maximum allowable position (yellow line in Fig. 11a).

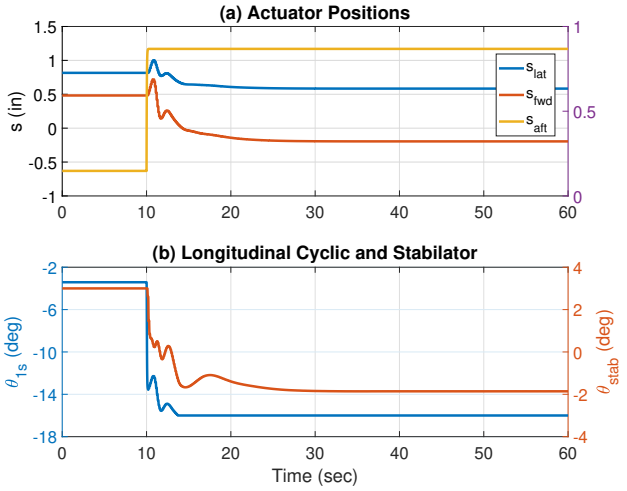

Figure 11. Time History of Actuator Positions, Longitudinal Cyclic and Stabilator for Maximum Aft Actuator Failure

As a result, both the lateral and forward actuators take up new trim positions. This causes the longitudinal cyclic (θ_{1s}) to become more negative and saturate at -16° (Fig. 11b) producing a nose-down pitching moment from the rotor. With the help of the pseudoinverse the controls are re-allocated to the working forward actuator and stabilator. A compensatory nose-up pitching moment is produced from the stabilator as it pitches down from 3° to -2°. It is important to note that although the redistributed pseudoinverse control allocation with the DI controller was able to compensate for the failed locked-in-place aft actuator at its allowable extreme position, the longitudinal cyclic has saturated and the rotor no longer has any control margin to produce additional nose-down moment. This lack of margin is not evident from the handling qualities metrics shown before, which show level 1 for this type of failure.

For aft actuator failure at the minimum allowable position (Fig. 12), the failure is modeled by moving the actuator down

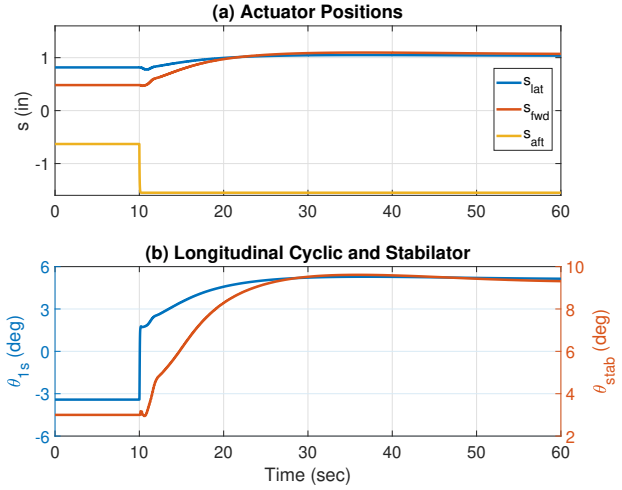

Figure 12. Time History of Actuator Positions, Longitudinal Cyclic and Stabilator for Minimum Aft Actuator Failure

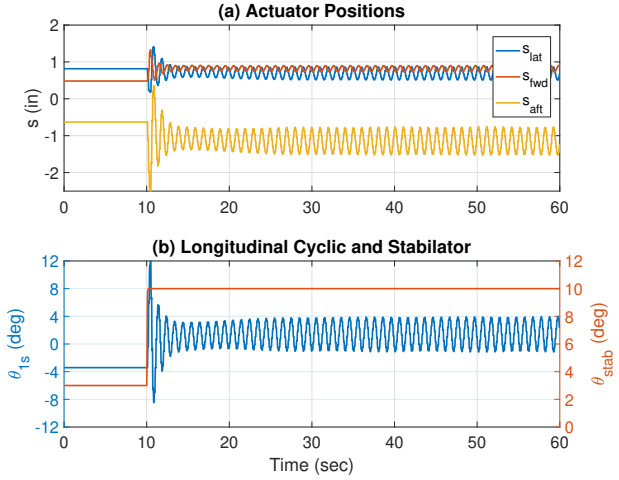

Figure 13. Time History of Actuator Positions, Longitudinal Cyclic and Stabilator for Maximum Nose-up Stabilator Position

by 0.93 inches (-0.63 in to -1.56 in) and locking it in place at 10 seconds (Fig. 12a). Figure 12b shows the resultant positive longitudinal cyclic (-3° to 5°) causing a nose-up pitching moment from the rotor which is then compensated by the nose-down moment from the stabilator (3° to 9°). Overall the response of the aircraft under minimum aft actuator failure is slower compared to the maximum aft actuator failure case. This is evident from the 15 and 25 seconds rise times of the stabilator response in the maximum and minimum aft actuator failure cases, respectively.

Stabilator Failure

Another possible damage scenario is the failure of the stabilator. Figures 13 and 14 represent the simulations of the maximum and minimum allowable locked stabilator failures according to the steady-state trim solutions (as shown in Table 3), respectively. Note that the case of maximum allowable stabilator failure has the worst stability margins (green diamond in Fig 5). At 10 seconds, the failure is simulated by moving the stabilator pitch to 10° pitch incidence (red line in Fig. 13b) and locking in place. This locked failure results in a stable response with limit cycle oscillations of the main rotor swashplate actuators (Fig. 13a) while maintaining a cruise speed of 150 knots (not shown here).

Meanwhile, for the case of minimum allowable stabilator failure, it is modeled by moving the stabilator pitch incidence to -8° at 10 seconds (shown by red line Fig. 14b). This results in a nose-up pitching moment from the stabilator. As a consequence, the longitudinal cyclic (θ_{1s}) becomes more negative and saturates at $-16°$ producing a compensatory nose-down pitching moment. Although the aircraft is stable after this failure scenario through the use of the redistributed pseudoinverse control allocation and DI controller, the aircraft now no longer has any control margin along the longitudinal axis because of the saturated longitudinal cyclic. This was not indicative in

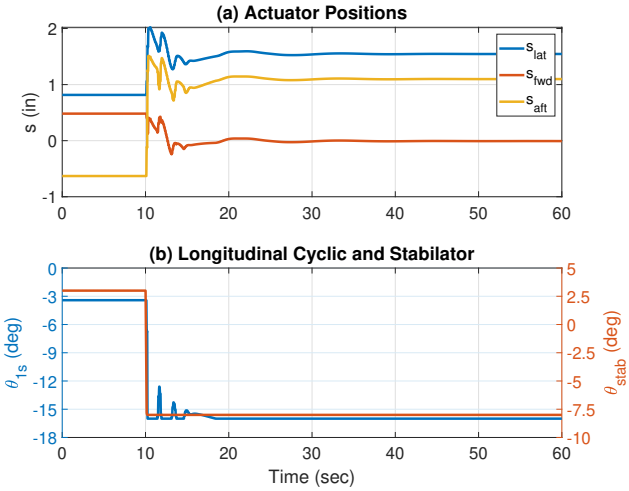

Figure 14. Time History of Actuator Positions, Longitudinal Cyclic and Stabilator for Minimum Nose-down Stabilator Position

the level 1 handling qualities metrics evaluated from the extracted linear models for this case.

Lateral Actuator Failure

Next, use of the ailerons as a redundant effector is examined in case of lateral actuator failure at a cruise speed condition of 150 knots. Figure 15a shows the time history of the lateral, forward and aft actuator positions from 0 to 60 seconds at a cruise speed of 150 knots with failure introduced at 10 seconds. The trim positions of the actuators prior to failure are shown from 0 to 10 seconds; at 10 seconds, the lateral actuator (s_{lat}) is moved by 0.3 inches (from 0.81 in to 1.11 in) and locked out of trim.

Post-failure, both the forward (s_{fwd}) and aft (s_{aft}) actuators do not deviate much from the pristine aircraft trim positions (as seen in Fig. 15a). As a result of the lateral actuator locking out

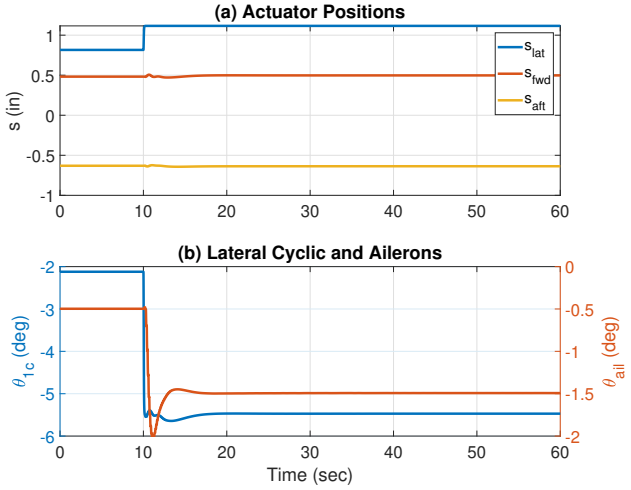

Figure 15. Time History of Actuator Positions, Lateral Cyclic and Ailerons for Lateral Actuator Failure

of trim, the lateral cyclic (θ_{1c}) becomes more negative moving from -2° to -5.5° (solid blue line in Fig. 15b) causing the main rotor to produce a roll-right moment.

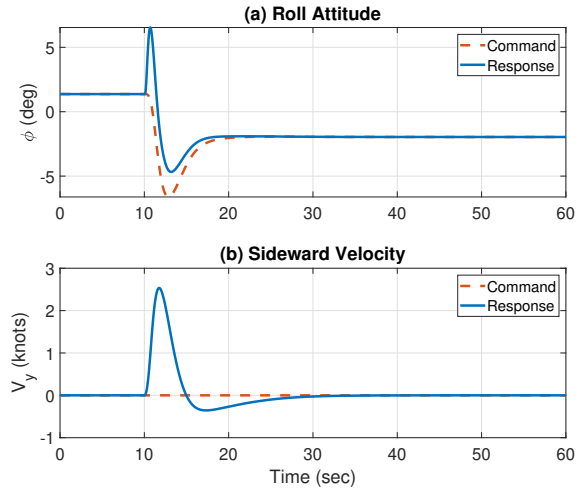

Figure 16. Time History of Roll Attitude and Sideward Velocity for Lateral Actuator Failure

Assuming that fault has been detected, the pseudoinverse is recalculated such that the it now reallocates additional lateral control authority to the ailerons. Hence, the ailerons (θ_{ail}) pitch differentially by 1° (from -0.5° to -1.5°, solid red line in Fig. 15b) to produce a compensatory roll-left moment. The roll-right moment from the main rotor due to the change in the lateral cyclic (θ_{1c}) causes a non-zero sideward velocity (as seen by solid blue line in Fig 16b). In order to maintain zero sideward velocity, the vehicle orients itself to a right wing up roll attitude (from 1.37° to -1.95°) as seen in Fig. 16a, which is enabled by the roll-left moment provided by the ailerons.

Maximum vs Minimum Tolerable Failures

Next, the aircraft response to allowable extreme lateral actuator failure conditions with pseudoinverse method is examined. Figures 17 and 18 represent the simulations for maximum and minimum allowable lateral actuator failure which were established from steady-state trim solutions (Table 3).

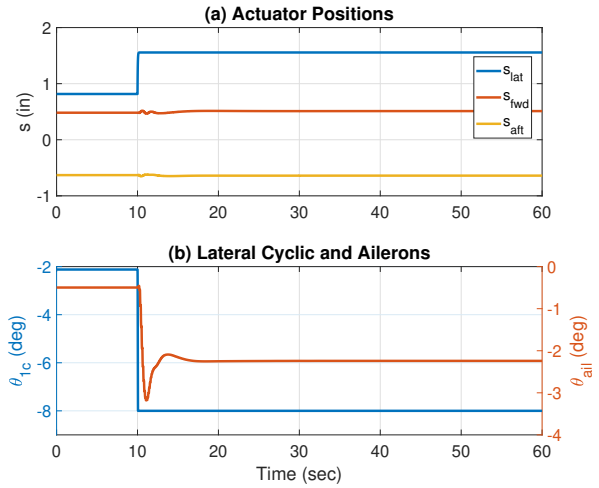

Figure 17. Time History of Actuator Positions, Lateral Cyclic and Ailerons for Maximum Allowable Lateral Actuator Failure

Figure 17a shows the time history of the main rotor swashplate actuators with the lateral actuator (s_{lat}) failure modeled by moving the actuator by 0.74 inches to its maximum allowable position of 1.55 inches (shown by blue line) and locking it at 10 seconds. This causes the lateral cyclic (θ_{1c}) to saturate at -8° (blue line in Fig. 17b) resulting in a roll-right moment from the main rotor which is then compensated by a roll-left moment produced by the ailerons, pitching differentially by -1.6° (from -0.5° to -2.1° shown by the red line in Fig. 17b).

Meanwhile, in case of the minimum allowable lateral actuator failure (Fig. 18) the locked failure is modeled by moving the lateral actuator (s_{lat}) by 1.31 inches (from 0.81 in to -0.5 in, blue line in Fig. 18a) and locking it out of trim at 10 seconds. The lateral cyclic (θ_{1c}) saturates at 8° (shown by blue line in Fig. 18b) producing a roll-left moment from the main rotor. This imbalance requires the aircraft to produce a compensatory roll-right moment from the ailerons, which move from -0.5° to 2.5° (red line in Fig. 18), enabled by the redistributed pseudoinverse control allocation method. In both cases, the aircraft retains lateral authority because of presence of the working ailerons with almost no degradation in roll bandwidth or phase delay while still maintaining level 1 handling qualities (Fig. 8).

Aileron Failure

Another potential point of failure along the lateral axis is failure of the ailerons. At 10 seconds, maximum allowable

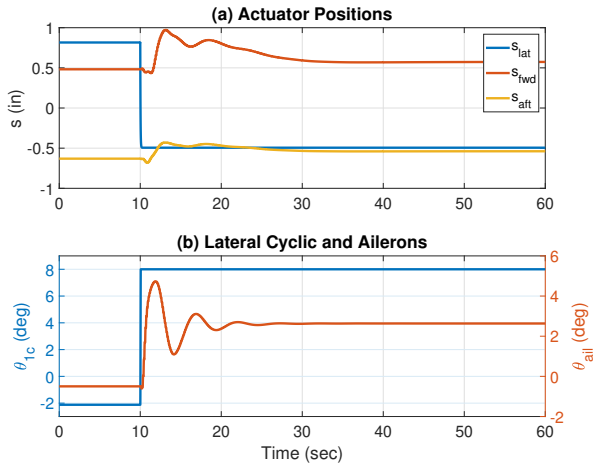

Figure 18. Time History of Actuator Positions, Lateral Cyclic and Ailerons for Minimum Allowable Lateral Actuator Failure

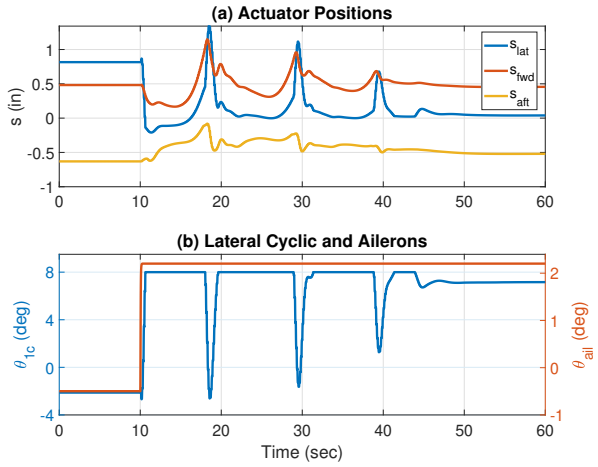

Figure 19. Time History of Actuator Positions, Lateral Cyclic and Ailerons for Maximum Allowable Aileron Failure

aileron failure, θ_{ail}, is modeled by pitching differentially by 2° and locking in place (red line in Fig. 19b). Post-failure, both the forward (s_{fwd}) and aft (s_{aft}) actuators do not deviate much from the pristine aircraft trim positions (as seen in Fig. 19a). As a consequence of the ailerons locking out of trim (from -0.5° to 2.2°) the wings produce a roll-right moment which is compensated by a roll-left moment from the main rotor enabled by the lateral cyclic (θ_{1c}) moving from -2.12° to 7° (blue line in Fig. 19) which is in turn achieved by moving the lateral actuator (s_{lat}) from 0.81 in to 0 in. Here, the nonlinear behavior in the transient response of the lateral cyclic is due to saturation.

As for the case of minimum allowable aileron failure (Fig. 20), the failure is modeled by pitching the ailerons differentially by -2° and locking it out of trim (red line in Fig. 20b). This results in a roll-left moment from the wings followed by a compensatory roll-right moment from the main rotor enabled by the lateral cyclic (θ_{1c}) moving from -2.12° to -8°.

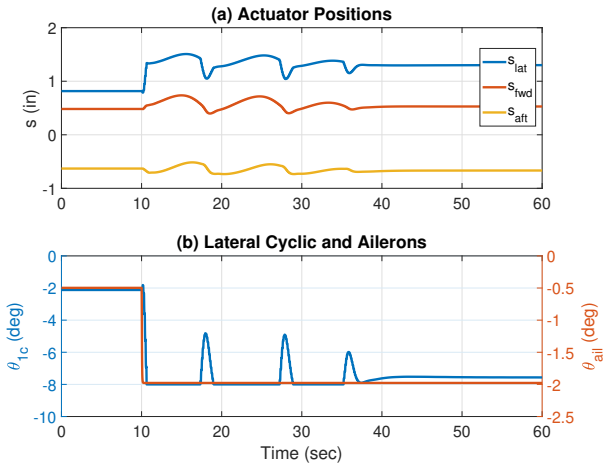

Figure 20. Time History of Actuator Positions, Lateral Cyclic and Ailerons for Minimum Allowable Aileron Failure

This is a mirrored response to what was observed in the previous case. Even though failure compensation is achieved using pseudoinverse control allocation and DI controller for both the minimum and maximum failure cases, this has led to the saturation of the main rotor lateral cyclic control resulting in a nonlinear behavior in the transient response of the aircraft. This saturation in the lateral cyclic (θ_{1c}) limits the aircraft from producing any additional lateral moment because of the lack of control margin. This is not evident from the roll axis handling qualities metrics (Figs. 8 and 7) which show some degradation but do not depart the level 1 boundary.

CONCLUSIONS

The present study proposes a pseudoinverse control allocation method on a compound helicopter in order to utilize the redundant control effectors in the feedback loop to compensate for locked-in-place actuator failures. It is shown to successfully compensate for actuator failures when the feedback control and the pseudoinverse control allocation method redistributes the control authority to the working actuators, assuming fault detection has taken place.

A range of allowable failures exist for all actuators from a steady state trim stand point at a cruise speed of 150 knots. Stability margins, phase delay, and bandwidth for the baseline and at the failure limit cases were examined for the longitudinal and lateral axis for a cruise speed of 150 knots. In the longitudinal axis, the aircraft stability margins remained level 1 for almost all failure limit cases with minimum failed aft actuator falling to level 2 and for failure at the maximum allowable stabilator nose-up position to level 3. It is also noted that the aircraft retains level 1 handling qualities for the pitch axis bandwidth with no significant changes post-failure. In the lateral axis, even post-failure, the evaluated handling qualities ratings remain level 1 for all types of failure considered.

Nonlinear simulations were conducted to examine the change in controls and aircraft response post-failure demonstrating

the capability of the redistributed pseudoinverse method. For aft actuator failure, the rotor is unable to produce any additional nose-down pitching moment at the maximum tolerable failure due to longitudinal cyclic saturation. Meanwhile, at the minimum tolerable failure the aircraft response is slower. This lack of control margin and sluggish response is not evident from the level 1 handling qualities metrics in the pitch axis for these types of failure. Simulation of stabilator failure at the maximum tolerable limit with level 3 stability margins show limit cycle oscillations. As for the case of minimum allowable stabilator failure, the aircraft loses all control margin in the longitudinal axis because of longitudinal cyclic saturation. This was not indicated in the level 1 handling qualities metrics evaluated.

From nonlinear simulations, lateral actuator failure is shown to be compensated for small and even maximum and minimum tolerable damage cases. The aircraft retains lateral authority due to the presence of the ailerons with level 1 handling qualities post-failure. However, in case of aileron failure at the maximum and minimum allowable failure limit, the lateral authority of the aircraft is lost due to the saturation of the main rotor lateral cyclic. This was not evident from the handling qualities metrics evaluated in the roll axis.

In summary, the pseudoinverse control allocation method is shown to perform well when failure is not at the actuator limits, and allows for an examination of control and aircraft response when failure occurs at the actuator limits. For failure at the actuator limits, it is noted that the handling qualities metrics evaluated from the extracted linear models do not indicate the substantial degradation in post-failure performance seen in nonlinear simulation (frequently showing level 1 handling qualities where nonlinear simulation shows control saturation, limit cycle oscillations, or sluggish response).

Author contact:
Praneet Vayalali vayalp@rpi.edu
Michael McKay mckaym2@rpi.edu
Farhan Gandhi fgandhi@rpi.edu

ACKNOWLEDGMENTS

This work is carried out at the Rensselaer Polytechnic Institute under the Army/Navy/NASA Vertical Lift Research Center of Excellence (VLRCOE) Program, grant number W911W61120012, with Dr. Mahendra Bhagwat as Technical Monitor. The authors would also like to acknowledge the Department of Defense and Army Research Office for sponsoring Mr. McKay through the National Defense Science and Engineering Graduate Fellowship.

REFERENCES

1. R. A. Eslinger and P. R. Chandler, "Self-Repairing Flight Control System program Overview," in *Proceedings of the IEEE 1988 National Aerospace and Electronics Conference*, pp. 504–511 vol.2, May 1988.

2. J. F. Stewart and T. L. Shuck, "Flight-Testing of the Self-Repairing Flight Control System Using the F-15 Highly Integrated Digital Electronic Control Flight Research Facility," tech. rep., NASA-TM-101725, 06 1990.

3. M. Bodson and J. E. Groszkiewicz, "Multivariable Adaptive Algorithms for Reconfigurable Flight Control," *IEEE Transactions on Control Systems Technology*, vol. 5, pp. 217–229, March 1997.

4. J. S. Brinker and K. A. Wise, "Flight Testing of Reconfigurable Control Law on the X-36 Tailless Aircraft," *Journal of Guidance, Control, and Dynamics*, vol. 24, no. 5, pp. 903–909, 2001.

5. R. Hess, "A Framework for Robust Rotorcraft Flight Control Design," *Journal of the American Helicopter Society*, vol. 56, pp. 22004–1, 04 2011.

6. M. W. Heiges, "Reconfigurable Controls for Rotorcraft—A Feasibility Study," *Journal of the American Helicopter Society*, vol. 42, no. 3, pp. 254–263, 1997.

7. R. Enns and J. Si, "Helicopter Flight-Control Reconfiguration for Main Rotor Actuator Failures," *Journal of guidance, control, and dynamics*, vol. 26, no. 4, pp. 572–584, 2003.

8. J. P. Reddinger and F. Gandhi, "Using Redundant Effectors to Trim a Compound Helicopter with Damaged Main Rotor Controls," in *American Helicopter Society 73rd Annual Forum Proceedings*, (Fort Worth, TX), May 2017.

9. P. Vayalali, M. Mckay, J. Krishnamurthi, and F. Gandhi, "Horizontal Stabilator Utilization for Post Swashplate Failure Operation on a UH-60 Black Hawk Helicopter," *Journal of the American Helicopter Society*, vol. 65, pp. 1–13(13), Apr. 2020.

10. P. Vayalali, M. Mckay, J. Krishnamurthi, and F. Gandhi, "Robust Use of Horizontal Stabilator in Feedback Control on a UH-60 Black Hawk," in *American Helicopter Society 75th Annual Forum Proceedings*, (Philidelphia, PA), May 2019.

11. D. Enns, "Control allocation approaches," in *Guidance, Navigation, and Control Conference and Exhibit*, p. 4109, 1998.

12. C. Ivler and O. Juhasz, "Evaluation of Control Allocation Techniques for a Medium Lift Tilt-Rotor," in *American Helicopter Society 71rd Annual Forum Proceedings*, (Virginia Beach, VA), May 2015.

13. T. Berger, O. Juhasz, M. J. S. Lopez, M. B. Tischler, and J. F. Horn, "Modeling and control of lift offset coaxial and tiltrotor rotorcraft," *CEAS Aeronautical Journal*, Aug 2019.

14. J. Krishnamurthi and F. Gandhi, "Flight simulation and control of a helicopter undergoing rotor span morphing," *Journal of the American Helicopter Society*, vol. 63, no. 1, pp. 1–20, 2018.

15. J. J. Howlett, "UH-60A Black Hawk Engineering Simulation Program. Volume 1: Mathematical Model," *NASA CR-166309*, 1981.

16. M. G. Ballin, "Validation of a Real-Time Engineering Simulation of the UH-60A Helicopter," *NASA TM-88360*, 1987.

17. D. A. Peters and N. HaQuang, "Dynamic Inflow for Practical Applications," *Journal of the American Helicopter Society*, vol. 33, pp. 64–66, Oct. 1988.

18. F. Bailey Jr, "A Simplified Theoretical Method of Determining the Characteristics of a Lifting Rotor in Forward Flight," *NACA Report 716*, 1941.

19. B. W. McCormick, *Aerodynamics, Aeronautics, and Flight Mechanics*. Wiley, second ed., Sept. 1994.

20. Moodie, A. M., and Yeo, H., "Design of a Cruise-Efficient Compound Helicopter," *Journal of the American Helicopter Society*, vol. 57, pp. 1–11, July 2012.

21. S. Goldstein, "On the Vortex Theory of Screw Propellers," *Proceedings of the Royal Society of London. Series A*, vol. 123, pp. 440–465, Apr. 1929.

22. J.-P. Reddinger and F. Gandhi, "Physics-based trim optimization of an articulated slowed-rotor compound helicopter in high-speed flight," *Journal of Aircraft*, vol. 52, no. 6, pp. 1756–1766, 2015.

23. "UH-60 Flight Control and Hydraulic Systems," Tech. Rep. 4747-9, U.S. Army Aviation War Fighting Center, Fort Rucker, AL, July 2002.

24. B. L. Stevens, F. L. Lewis, and E. N. Johnson, *Aircraft Control and Simulation: Dynamics, Controls Design, and Autonomous Systems*. John Wiley & Sons, 2015.

25. M. B. Tischler, T. Berger, C. M. Ivler, M. H. Mansur, K. K. Cheung, and J. Y. Soong, *Practical Methods for Aircraft and Rotorcraft Flight Control Design: An Optimization-Based Approach*. Reston, VA: AIAA Education Series, 2017.

26. M. Bodson, "Evaluation of optimization methods for control allocation," *Journal of Guidance, Control, and Dynamics*, vol. 25, no. 4, pp. 703–711, 2002.

27. T. A. Johansen and T. I. Fossen, "Control allocation—a survey," *Automatica*, vol. 49, no. 5, pp. 1087–1103, 2013.

28. Anon, "Flight Control Systems—Design, Installation, and Test of Piloted Military Aircraft, General Specification for SAE-AS94900," tech. rep., SAE International, Warrendale, PA, USA, July 2007.

29. Anon, "Handling Qualities Requirements for Military Rotorcraft," tech. rep., Aeronautical Design Standard and Performance, Specification ADS-33E-PRF, US Army Aviation and Missile Command, 2000.